Signature of Ocean Warming at the Mixed Layer Base

Louis Clément[1], **Elaine L. McDonagh**[1,2], **Alice Marzocchi**[1], **A. J. George Nurser**[1]

[1]National Oceanography Centre, Southampton, United Kingdom

[2]NORCE, Norwegian Research Centre, Bjerknes Centre for Climate Research, Bergen, Norway

Key Points:

- Temperature changes at the winter mixed layer base are partitioned into heave and spice contributions.
- Isopycnal heave explains multidecadal warming in subtropical gyres at the winter mixed layer base.
- Density-compensated temperature anomalies originate in regions of surface salinity maxima.

Corresponding author: Louis Clément, `l.clement@noc.ac.uk`

This article has been accepted for publication and undergone full peer review but has not been through the copyediting, typesetting, pagination and proofreading process, which may lead to differences between this version and the Version of Record. Please cite this article as doi: 10.1029/2019GL086269

Abstract

The warming climate influences the ocean by changing its wind-driven dynamics and by inputting extra heat. This study analyzes the warming where temperature anomalies penetrate the ocean interior, i.e. by focusing on the winter mixed layer (WML) base. This allows to distinguish regions where ocean circulation contribute to warm anomalies from locations where density-compensated temperature anomalies locally enter the ocean along isopycnals. Multidecadal (1980-2018) local temperature trends from a hydrographic dataset are examined at the WML base, and partitioned into components relating to isopycnal movement (heave) and change along isopycnals (spice). Subtropical gyres and western boundary currents show warming larger than the global average that mostly projects onto heave. This is the result of the strengthening of the circulation in the Southern Hemisphere subtropical gyres, and is related to both wind-driven changes and Southern Ocean warming. Subtropical regions of surface salinity maxima are influenced by warm anomalies along isopycnals.

Plain Language Summary

This study analyses the warming of the ocean specifically where temperature changes penetrate the ocean interior. To do so, we analyse the temperature at the depth just below the layer that directly interacts with the atmosphere. This allows us to establish whether the wind-driven circulation is more important than the surface heat and freshwater fluxes in controlling the subsurface temperature changes. Using observations taken from 1980 to 2018, we establish that west of the subtropical ocean basins, wind-driven circulation controls subsurface temperature whereas in regions where surface salinity is highest, temperature anomalies penetrate the ocean along with salinity differences. Our work highlights the contrast between these two processes by which warmer water enters the ocean. These results are useful to understand regional ocean heat content because they help to distinguish between temperature anomalies of the ocean interior that originate from changes of surface heat and freshwater fluxes from those that result from wind changes.

1 Introduction

The ocean absorbs up to 93% of the warming in the Earth's climate system [*Levitus et al.*, 2012]. Although the net ocean warming is driven by air-sea flux perturbations, the water exchange across the mixed layer base through subduction is a key stage in ocean heat uptake. This exchange isolates the water mass from the atmosphere and facilitates the oceanic storage of heat. The size of the uptake across the mixed layer base is set by the combination of the exchange strength and the water properties that participate in that exchange. Although the global ocean warming of the upper layer has been extensively studied [*Roemmich et al.*, 2015], as well as the regional subduction strength, such as in the Southern Ocean [*Sallée et al.*, 2010], the evolution of water mass properties at the mixed layer base (the depth relevant to heat uptake in the ocean interior) is less well understood.

Water mass properties at the base of the mixed layer are not only influenced by changes in air-sea fluxes, but also by circulation and mixing variability. Focusing on this depth should help to distinguish temperature variability due to changes of wind-driven circulation [*Huang*, 2015] from those due to changes of subducted rates [*Marshall et al.*, 1993]. Subduction of temperature anomalies from the mixed layer into the ocean interior occurs through vertical and horizontal advection [*Woods*, 1985], changes in mixed-layer depth, and diffusion at the mixed layer base [*Robbins et al.*, 2000; *Yeager and Large*, 2007], which can affect non-outcropping isopycnals. Changes of temperature and salinity on isobars may be partitioned between their diabatic changes on isopycnals (spice) and their adiabatic changes due to isopycnal displacements (heave). This separation aims at isolating subsurface anomalies due to surface buoyancy flux variability from wind-induced changes [*Bindoff and McDougall*, 1994].

Surface changes affect spice and heave differently depending on the timescales involved. On multi-decadal scales, heave mainly arises from isopycnal deepening of subtropical mode waters as a result of surface warming followed by subduction [*Church et al.*, 1991; *Häkkinen et al.*, 2016]] rather than downward heat diffusion. Subsurface multi-decadal cooling and freshening on isopycnals, spice, compensates some of the warming heave on the poleward sides of subtropical gyres in regions of stabilizing temperature (decreasing with depth) and destabilizing (decreasing with depth) salinity [*Durack and Wijffels*, 2010; *Häkkinen et al.*, 2016]. These salinity anomalies result not only from changes in surface freshwater fluxes, but also from long-term warming that drives the poleward displacement of isopycnals towards regions of different surface salinity. This isopycnal displacement mostly represents isotherm displacement except in subpolar regions [*Lago et al.*, 2016]. Although changes in low-frequency ocean dynamics and wind stress also affect multidecadal changes in temperature, their impacts are particularly strong on interannual-decadal variability. Wind changes associated with climate oscillations and planetary waves are the main drivers of the interannual-decadal heave variability [*England et al.*, 2014; *Evans et al.*, 2017; *Piecuch et al.*, 2017].

To establish where warm anomalies enter the ocean, we focus on the property variability at the maximum mixed layer depth that varies in space but not in time (Fig. 1a). This depth captures the winter mixed layer properties that subduct into the interior and avoids the intense mixed layer seasonal cycle, which is less relevant on multidecadal scales. We examine the property variability using a spice and heave framework. We also interpret property changes as pure heave, pure warming and pure freshening to establish the dominant forcing [*Bindoff and McDougall*, 1994]. In addition, we examine the stratification of the water column both in terms of temperature and salinity. The stratification or preconditioning of the water column, which is affected by circulation changes, colludes with the surface forcing perturbation to set the perturbed mixed layer properties. In the discussion, we relate our results at the winter mixed layer base to candidate forcing mechanisms of subsurface properties displayed on isobaths or isopycnals in the context of previous studies.

2 Data and Methods

The monthly mixed layer depth is calculated between 1980 and 2018 using the variable density threshold associated with a 0.2°C decrease in temperature [*Holte et al.*, 2017] in the objectively analysed EN4 data set [*Good et al.*, 2013]. We undertake our analysis using conservative temperature Θ and absolute salinity S, converted from the EN4 potential temperature and practical salinity. At each 1° gridpoint, which is the EN4 spatial resolution, the maximum mixed layer depth is chosen as the depth of analysis –this represents the maximum winter mixed layer depth or WML base. Spice and heave anomalies of Θ and S are calculated at the WML base.

The spice anomaly, denoted by $\Theta'|_n(t,z)$, is evaluated by comparing the temperature at time t on a density surface $\gamma^n(t,z)$, denoted by $\Theta(t,z)$, with the temperature on the same density surface at a reference time t_0, denoted by $\Theta(t_0, z_0[\gamma^n(t,z)])$. The residual between temperature on isobars, $\Theta'|_z(t,z)$, and the spice, $\Theta'|_n(t,z)$, represents the heave, $\Theta'|_h(t,z)$ [*Doney et al.*, 2007]; this approach avoids residuals arising from the linearization of a background $\partial_z\Theta$ in the original decomposition [*Bindoff and McDougall*, 1994]. The spice and heave components of temperature anomalies (similarly for salinity) become:

$$\Theta'|_n(t,z) = \Theta(t,z) - \Theta(t_0, z_0[\gamma^n(t,z)]),$$
$$\Theta'|_h(t,z) = \Theta(t_0, z_0[\gamma^n(t,z)]) - \Theta(t_0, z), \quad (1)$$

with the reference profile $\Theta(t_0, z_0)$ taken as a 'summer' profile defined from the lowest density at the shallowest pressure (5 dbar). Choosing this summer profile ensures the existence in the reference profile of the density surface at the WML base. The anomaly on isobars is the sum of the two components

$$\Theta'|_z(t,z) = \Theta(t,z) - \Theta(t_0,z) = \Theta'|_n(t,z) + \Theta'|_h(t,z). \quad (2)$$

Trends of (total, spice and heave) temperature changes at the WML base are calculated using linear least-squares regression (Fig. 2).

In order to relate WML base temperature evolution to changes in surface forcing (heat flux, evaporation minus precipitation and wind stress) the property changes are decomposed into three pure processes [*Bindoff and McDougall*, 1994; *Vaughan and Molinari*, 1997]: pure warming, pure freshening and pure heave (W, F and H in Fig. 1d–f). The formulation of these pure processes is calculated from the spice/heave decomposition, the definition of neutral surfaces, γ^n: $\alpha\Theta'|_n = \beta S'|_n$, and the density ratio (R_ρ=$\alpha\partial_z\Theta/\beta\partial_z S$). The thermal expansion, α, and saline contraction, β, coefficients are $\alpha = -\rho^{-1}\partial\rho/\partial T$ and $\beta = \rho^{-1}\partial\rho/\partial S$. In the pure warming scenario ($\alpha\Theta'|_z > 0$ and $\beta S'|_z = 0$; grey to red diamonds in Fig. 1d–f), salinity anomalies are related through

$$\beta S'|_n = -\beta S'|_h. \quad (3)$$

The pure freshening scenario ($\alpha\Theta'|_z = 0$ and $\beta S'|_z < 0$; grey to green diamonds in Fig. 1d–f) relates temperature anomalies through

$$\alpha\Theta'|_n = -\alpha\Theta'|_h, \quad (4)$$

whereas pure heave ($\alpha\Theta'|_n = \beta S'|_n = 0$; movement along Θ/S curves in Fig. 1d–f) relates temperature anomalies through

$$\alpha\Theta'|_z = \alpha\Theta'|_h. \quad (5)$$

These can be thought of as the temperature and salinity changes if the only forcing were one of these pure processes. There are two approaches to estimating the relative importance of these three processes. The inverse approach solves an underdetermined linear system obtained from the spice and heave decomposition of temperature and salinity, and estimates simultaneously the three pure processes using a singular value decomposition [*Bindoff and McDougall*, 1994]. In our study, which applies the decomposition of pure processes to regional areas at the WML base as opposed to longitudinal transects [*Bindoff and McDougall*, 1994], this inverse approach (not shown) appeared biased towards pure freshening arising from the large spatial variability of the density ratio when compared with the components of Eq. 2. Here, we use the method described in [*Vaughan and Molinari*, 1997] and quantify the variance explained, R^2, of each pure process at the WML base of each region using the total, the spice, and the heave trends of Θ and S. Only two pure processes coexist at Θ/S maximum and minimum [*Bindoff and McDougall*, 2000] and only pure heave exists for $R_\rho = 1$. However, determining the strength of the three pure processes while removing locations with large R_ρ (above the highest 69% percentile) or R_ρ within [-1.0,1.0] or [0.9,1.1] does not significantly affect our results, suggesting the absence of bias in our method.

We examine the stratification patterns of the water column through two parameters, the Turner angle and the density ratio. The Turner angle (Fig. 1b), Tu, quantifies the density compensation of the vertical gradients of temperature and salinity [*Ruddick*, 1983], $\mathrm{Tu} = \tan^{-1}[(\alpha\partial_z\Theta + \beta\partial_z S)/(\alpha\partial_z\Theta - \beta\partial_z S)]$. Equivalently, the density ratio (Fig. 1b), $R_\rho=\alpha\partial_z\Theta/\beta\partial_z S=\frac{\partial\Theta}{\partial S}/\frac{\partial\Theta}{\partial S}|_n$, compares the slope of the Θ-S curve with a local isopycnal and relates to Tu via $R_\rho = -\tan(\mathrm{Tu}+45)$ (Fig. 1c). A steeper Θ-S slope than the local isopycnal occurs for $R_\rho > 1$ (Fig. 1d). The vertical gradients used to calculate Tu are estimated over the ML base for the three winter months (Fig. 1b). One of the advantages of Tu over R_ρ [*Ruddick*, 1983] is that it has a well-defined transition value (45°) instead of infinity when moving from regions with subsurface to surface salinity maximum. We identify high-Tu regions (Tu>55°) where coherent patterns of density compensating anomalies are more likely to subduct into the interior [*Yeager and Large*, 2004].

Western boundary current regions and subtropical gyres are isolated to examine the mixed layer property evolution over coherent circulation regimes. The anticyclonic circulation of subtropical gyres have the largest dynamic height signature (integrated from 2000 to 200 m). Subtropical gyres are localized through their circulation strength; we retain regions with a dynamic height in the highest 80% percentile (dashed lines in Fig. 2 panels). Western boundary currents (the Kuroshio Current, the Gulf Stream, the Eastern Australian Current, the Brazil Current and the Agulhas Current) are identified using a latitude-longitude box following *Wu et al.* [2012], who studied surface warming within boundary currents.

3 Results

3.1 Topography of the mixed layer base

The WML base (Fig. 1a) is deepest in the North Atlantic, specifically in the subpolar Greenland, Iceland, Norwegian and Labrador Seas and also in the Sargasso Sea and eastern North Atlantic. Deep WMLs also emerge in the southern sectors of the Indian and Pacific Oceans at 40-60°S where formation of Subantarctic Mode Water SAMW occurs [*McCartney*, 1977, 1982]. Deep winter mixed layers are generally associated with localized regions of subtropical and subpolar mode water formation [*Talley*, 1999].

3.2 Stratification at the mixed layer base

Away from the poles, the Turner angle across the WML base (Fig. 1b) tends to be greater than -45°, reflecting a stabilizing temperature structure as temperature increases towards the surface. This is consistent with a system where surface waters warm at the equator and transition to cooling near the poles. Within these regions away from the poles (Tu>-45°), salinity may decrease towards the surface |Tu|<45° or increase towards the surface Tu>45°. Where |Tu|<45° (Fig. 1e), there is a subsurface salinity maximum at/below the WML base and the regions tend to be associated with areas where precipitation dominates over evaporation. Where Tu>45° (Fig. 1d), both salinity and temperature increase towards the surface, the thermocline is nearly density compensating and regionally evaporation dominates over precipitation. These regions (dark purple in Fig. 1b) largely represent the evaporative regimes of subtropical gyres. Where Tu<-45°, in the high-latitude Southern Ocean and Labrador Sea, depth-increasing salinity has a stronger effect on density than depth-increasing temperature due to reduced α at cold temperature (Fig. 1f).

3.3 Multidecadal temperature variability at the mixed layer base

Globally, warming prevails at the WML base on multidecadal time scales, except over the eastern Pacific (Fig. 2a), the tropical Indian and Atlantic oceans and parts of the Southern Ocean. Subtropical gyres (dashed lines in Fig. 2) warm on average by 11.7±0.1 m°C yr^{-1} with a large contribution from western boundary currents (black boxes in Fig. 2) (14.4±0.2 m°C yr^{-1}) that partly overlap with the gyres. This reflects the large subtropical warming compared with the global ocean average, 6.1±0.2 m°C yr^{-1} (Fig. 3a). The heave component dominates the warming of the western subtropical Pacific, the North Atlantic and the southeast Indian Ocean as well as the cooling of the eastern tropical Pacific. For example, the region-averaged variance explained by a linear trend for the heave is 70% for the western sub-tropical/tropical Pacific (equatorward of 40° and westward of 120°W) as opposed to 4% for the spice. This volume-averaged warming of the WML (0.26°C) is larger than the warming below (0.16°C) measured from the WML base to 700 m, which corresponds to the 99.5% percentile of the global WML base (Fig. 1a).

Gyres and western boundary currents show a warming trend largely attributed to their heave component (Fig. 3a). The spice, however, dominates the warming of the North Atlantic western boundary current and is mostly positive in gyres, which reinforces their heave warming. Comparing the relative strength of the three pure processes (Fig. 3b) reveals that pure heave prevails in western boundary currents whereas no single process seems to dominate in gyres. The largest contribution of the heave component for boundary currents is consistent with the prevalent wind-driven dynamics attributed to the warming of boundary currents [*Wu et al.*, 2012].

High-Tu regions such as the North Atlantic and the southeast Pacific correspond to surface salinity maxima where the hydrological cycle has intensified in recent decades [*Capotondi et al.*, 2012]. These are characterised by generally opposite spice and heave in individual basins (see the basin markers in Fig. 3a), which contributes to a net warming of these regions by 7.2±0.1 m°C yr^{-1} (Fig. 3a). Spice warming opposing the cooling heave is evident in some high-Tu regions (Tu>55°) such as the South Atlantic, and the southeast Pacific, but more frequently, cooling spice compensates warming heave e.g. in the North Pacific and in the southeast Indian Ocean (Fig. 2b and c). The spice trend at the WML base and its spatial structure (Fig. 2b) mostly agree with previously described ~50-60 yr trends of temperature (or salinity) on outcropping isopycnals, confirming the pertinence of our results over longer periods. For example, the freshening (cooling) of the North Pacific around 30°N and of the Southern Ocean around 30-50°S (Fig. 2b) appeared in the same regions on γ^n=25 or 26.75-27 kg m^{-3}, respectively [*Durack and Wijffels*, 2010; *Häkkinen et al.*, 2016].

Decomposing $\alpha\Theta'$ and $\beta S'$ reveals large salinity changes on isopycnals in the high-Tu South Atlantic that are not fully compensated in heave (Fig. S7d vs f) as opposed to Θ, which results in large total salinity changes (Fig. S7b). The decomposition into the three pure processes (Fig. 3b) unveils the large contribution of pure warming and pure freshening (for Tu>55°) that is expected in the presence of spice injections associated with heave, potentially due to wind-induced upwelling. An example of coupling between spice injections and the presence of heave around the mixed layer base was presented by *Yeager and Large* [2007] (their Fig.11). In the tropical western Pacific, the negative heave in salinity coupled with the positive heave in temperature is consistent with the shallow downwelling above the subsurface salinity maximum in this region of increasing Θ and decreasing S towards the surface. This coupling must relate to the accelerated Pacific trade winds observed over 1992-2011 [*England et al.*, 2014].

The Southern Ocean from 40 to 60°S reflects large positive heave counterbalanced by cooling spice (Fig. 3a). The heave component does not strongly vary across the Indo-Pacific section compared with the South Atlantic where the boundary current dominates (Fig. 2c). The warm heave at 40-60°S (Fig. 2c) relates to the multidecadal isopycnal deepening of subtropical and subpolar mode waters around σ_0 = 26.0–27.6 kg m^{-3} that spreads equatorward (Fig. S4 left) from their ventilation regions, where the deepening is maximal [*Häkkinen et al.*, 2016]]. These mode waters include the Subantarctic Mode Waters SAMW (σ_0 = 26.0–27.0 kg m^{-3}) and the Antarctic Intermediate Water AAIW (σ_0 = 27.0–27.5 kg m^{-3}) that are formed from the upwelled deep waters modified at the surface. The maximal heave from isopycnal deepening around σ_0 = 27.0 kg m^{-3} reflects the volume increase of SAMW associated with a volume decrease of AAIW. Pure heave is the dominating process in the Southern Ocean (Fig. 3b) whereas pure warming and pure freshening are indistinguishable. Despite no net warming (Fig. 3a) and the large contribution of pure heave only (Fig. 3b), the warming heave and cooling spice of the Southern Ocean (Fig. 3a) are consistent with subduction following surface warming [*Church et al.*, 1991].

3.4 Data sparseness and robustness of the results

Sparse sampling during the pre-Argo era of temperature and salinity profiles in the Southern Hemisphere and specifically in the Southern Ocean [*Abraham et al.*, 2013; *Rhein et al.*, 2013] might bias EN4 trends by over-representing an inadequate climatology and misrepresenting isopycnals at the WML base. The EN4 temperature and salinity observational weights that characterise the strength of observational measurements [*Good et al.*, 2013] allow detection of regions of sparse data coverage where trends on isopycnals might be affected by the addition of Argo (Section S1). Such regions with low temperature and salinity observational weights appear mainly in the southeastern Pacific and the Southern Ocean (white regions in Fig. 2). In addition, given that approximately three times fewer salinity profiles were sampled in the pre-Argo era than temperature profiles [*Rhein et al.*, 2013], regions affected by low salinity sampling appear in the midlatitudes of the southwestern Pacific and in the North Pacific (white regions in Fig. 2).

Analysing the monthly ocean state estimate (Simple Ocean Data Assimilation SODA v3.7.2, *Carton et al.* [2018]) and another objectively-mapped gridded dataset with a drastically lower pentadal temporal resolution (NODC, *Levitus et al.* [2012]) confirms the overall robustness of temperature trends of the subtropical WML base (Fig. S6). This robustness is further confirmed by studying the interannual-decadal variability of temperature anomalies (Section S2) and by changing the ML definition (Section S3). SODA, which improves the representation of the undersampled Southern Ocean and also smooths the Argo transition [*Häkkinen et al.*, 2016], partly reinforces the observation of cooling spice and warming heave observed in the Indian and Pacific sectors of the Southern Ocean despite the low data coverage in EN4. Regardless of the reduced observational coverage over the pre-Argo era of the high-Tu southeast Pacific and to a lesser extent of the South Atlantic (white regions in Fig. 2), the signs of spice and heave trends for the pre-Argo era (Fig. S5) roughly agree with Fig. 2. Along with the SODA analysis, this suggests that the Argo transition might amplify the trends of these regions with poor data coverage (Fig. 2). Equatorward of 20°N and 20°S, where the spice and heave trends are weaker than in the subtropics, regional patterns appear less consistent within the three products.

4 Discussion

Having described temperature trends at the depth where subduction occurs, we consider potential mechanisms for the regional patterns of those trends. The zonal asymmetry of $\Theta'|_z$ in the tropical Pacific (Fig. 2a) and its mid-latitude increase is reminiscent of the Pacific Decadal Oscillation and the resulting temperature changes from wind stress anomalies. The westward acceleration of the trade winds during 1992–2011 contributes to the enhanced upwelling and cooling in the eastern tropical Pacific as well as to the accumulation of heat in the subsurface Indian and western tropical Pacific Oceans [*Roemmich et al.*, 2015] subsequent to Ekman-divergence at the Equator [*England et al.*, 2014]. Wind stress anomalies also spin-up the subtropical Pacific gyres [*Qiu and Chen*, 2012; *Roemmich et al.*, 2016] and displace isopycnals downward ($\Theta'|_h > 0$) for example around 170°W 40°S [*Roemmich et al.*, 2007]. This is consistent with an amplified Ekman pumping due to wind-driven convergence [*Roemmich et al.*, 2016] over the last decades. The enhanced tropical upwelling and the subtropical gyre intensification agree with the negative and positive heave identified east and west of 120°W, respectively, in the Pacific (Fig. 2c) despite our longer period of observations.

The wind stress poleward shift and intensification –due to varying Southern Annular Mode–coupled with increased surface heat flux [*Cai et al.*, 2010] contributes to warming the southern subtropical gyres [*Gao et al.*, 2018]. Therefore, the warming $\Theta'|_z$ at the WML base around 30–50°S in the Indian and Southwest Pacific, that is mostly represented by its heave component, is consistent with a wind-driven redistribution of heat associated with a changing heat flux south of this latitudinal section. Another mechanism for warm heave alongside spice cooling without changing winds is the equatorward Ekman transport of warmed surface waters that subsequently subduct on lighter isopycnals and mix with warmer and saltier water parcels [*Church et al.*, 1991; *Häkkinen et al.*, 2016]. This should result in cooling spice for $R_\rho > 1$ (Fig. 1d) —south of and around Australia (Fig. 1b)— whereas cooling spice also appear further south poleward of 50°S (Fig. 2b). Other explanations such as the southward shift of the Antarctic Circumpolar Current [*Alory et al.*, 2007] can explain the freshening of spice anomalies around 50°S [*Durack and Wijffels*, 2010]. Alternatively, increased precipitation would also result in freshening and cooling along isopycnals where R_ρ<0 (Fig. 1e).

The temperature anomaly that mainly projects onto heave (Fig. 2) follows the overall warming at the surface with cooling of the subtropical-tropical eastern Pacific over recent decades (*Yang et al.* [2016] their Fig. 3a). The enhanced warming of western boundary currents (Fig. 3a), 2-3 times greater than the global average, agrees with findings at the surface over the past century [*Wu et al.*, 2012]. The potentially wind-driven mechanisms responsible for this enhanced warming may involve poleward migration or intensification of these boundary currents [*Wu et al.*, 2012].

Both varying freshwater fluxes and isopycnal movement due to anthropogenic warming contribute to salinity changes on isopycnals [*Durack and Wijffels*, 2010]. Equivalently, warming on isopycnals coexists assuming smaller poleward displacement of isopycnals than isotherms [*Gille*, 2002]. Because isopycnal trends occur over high-Tu regions (Fig. 2b), instead of regions with positive poleward gradients of surface salinity (i.e. from 10 to 20°S in the south Atlantic), spice injections [*Yeager and Large*, 2007] or varying subduction processes [*Luo et al.*, 2005] may participate in these patterns on multidecadal scales in addition to the interannual-decadal scales [*Kolodziejczyk and Gaillard*, 2012]. With weak stratification and destabilizing salinity, spice injections can occur in winter through large diapycnal diffusion of heat and salt resulting from increased Θ and S gradients at the base of the WML without changing the buoyancy fluxes. Spice injections can arise from winter convective boundary layer mixing and double-diffusive salt fingers [*Johnson*, 2006; *Yeager and Large*, 2007]. Enhanced Θ and S gradients develop not only as a result of changing surface fluxes [*Capotondi et al.*, 2012] but also from the advection of cold water masses under the WML base, as suggested by the cool heave in these regions described above.

5 Conclusions

We have focused on the temperature evolution at the WML base, where permanent subduction occurs. Doing so has allowed us to distinguish high-Tu regions (with mostly opposing spice and heave per basin) from gyre circulation (with mostly positive spice and heave), while confirming the relevance of subtropical latitudes in the warming ocean [*Levitus et al.*, 2012]. Such a distinction no longer persists when considering the top 700 m, as for example in the Southern Hemisphere which becomes dominated by the positive heave and cooling spice of subpolar mode waters [*Häkkinen et al.*, 2016; *Desbruyères et al.*, 2017], or when focusing at a constant depth [*Doney et al.*, 2007] that can only partly capture the depth-varying spice injection. In contrast to previous studies on spice and heave [*Durack and Wijffels*, 2010; *Häkkinen et al.*, 2016], our results emphasize the relevance of a net warming despite the strong opposing spice and heave for isopycnals that outcrop in high-Tu regions. Moreover, focusing on the WML base reveals that both spice and heave contribute to warmer western boundary currents and subtropical gyres during our period of study.

The present analysis allows to simultaneously display regional patterns of spice and heave that appear in regions of shallow WML base (high-Tu regions, tropical oceans, subtropical gyres) and in regions of deep WML base (in the North Atlantic and the Southern Ocean around 30-50°S downstream of ventilation regions at 50°S). By identifying temperature anomalies that subduct simultaneously at varying depths, we will generate in future work a new set of boundary conditions based on the spice and heave decomposition to be applied to advective/diffusive circulation instead of using sea surface temperature [*Zanna et al.*, 2019]. For instance, spice anomalies broadly follow the equatorward and westward geostrophic pathways along isopycnals [*Luyten et al.*, 1983], whereas heave anomalies will affect the circulation. This way, we could attempt to partition temperature anomalies into excess heat that enters the ocean due to top-of-atmosphere temperature imbalance or into heat advected by circulation changes [*Gregory et al.*, 2016].

Acknowledgments

L. C. thanks Trevor McDougall for stimulating discussions on the spice and heave decomposition. This study benefited from discussions with Brian King, Harry Bryden, Yvonne Firing and Rachel Killick. The manuscript was significantly improved by the comments of three anonymous reviewers. The present work was funded by the NERC project (NE/P019293/1) Transient tracer-based Investigation of Circulation and Thermal Ocean Change (TICTOC).

The EN4 dataset version EN.4.2.1 is provided by the Met Office Hadley Centre at https://www.metoffice.gov.uk/hadobs/en4/download.html. The Simple Ocean Data Assimilation SODA v3.7.2 is provided by the University of Maryland and Texas A&M University and can be accessed at http://dsrs.atmos.umd.edu/DATA/soda3.7.2/REGRIDED/ocean. The NOAA-NODC database can be accessed at https://www.nodc.noaa.gov/OC5/3M_HEAT_CONTENT.

References

Abraham, J. P., M. Baringer, N. L. Bindoff, T. Boyer, L. J. Cheng, J. A. Church, J. L. Conroy, C. M. Domingues, J. T. Fasullo, J. Gilson, G. Goni, S. A. Good, J. M. Gorman, V. Gouretski, M. Ishii, G. C. Johnson, S. Kizu, J. M. Lyman, A. M. Macdonald, W. J. Minkowycz, S. E. Moffitt, M. D. Palmer, A. R. Piola, F. Reseghetti, K. Schuckmann, K. E. Trenberth, I. Velicogna, and J. K. Willis (2013), A review of global ocean temperature observations: Implications for ocean heat content estimates and climate change, *Reviews of Geophysics*, *51*(3), 450–483.

Alory, G., S. Wijffels, and G. Meyers (2007), Observed temperature trends in the Indian Ocean over 1960–1999 and associated mechanisms, *Geophys. Res. Lett.*, *34*, L02,606.

Bindoff, N. L., and T. J. McDougall (1994), Diagnosing climate change and ocean ventilation using hydrographic data, *J. Phys. Oceanogr.*, *24*, 1137–1152.

Bindoff, N. L., and T. J. McDougall (2000), Decadal changes along an Indian Ocean section at 32°S and their interpretation, *J. Phys. Oceanogr.*, *30*, 1207–1222.

Cai, W. J., T. Cowan, S. Godfrey, and S. Wijffels (2010), Simulations of processes associated with the fast warming rate of the southern midlatitude ocean, *J. Clim.*, *23*, 197–206.

Capotondi, A., M. A. Alexander, N. A. Bond, E. N. Curchitser, and J. D. Scott (2012), Enhanced upper ocean stratification with climate change in the CMIP3 models, *J. Geophys. Res.*, *117*, C04,031.

Carton, J. A., G. A. Chepurin, and L. Chen (2018), SODA3: a new ocean climate reanalysis, *J. Clim.*, *31*, 6967–6983.

Church, J. A., J. S. Godfrey, D. R. Jackett, and T. J. McDougall (1991), A model of sea level rise caused by ocean thermal extension, *J. Clim.*, *4*, 438–456.

Desbruyères, D., E. L. McDonagh, B. A. King, and V. Thierry (2017), Global and full-depth ocean temperature trends during the early 21st century from Argo and repeat hydrography, *J. Clim.*, *30*, 1985–1997.

Doney, S., S. Yeager, G. Danabasoglu, W. G. Large, and J. C. McWilliams (2007), Mechanisms governing interannual variability of upper-ocean temperature in a global ocean hindcast simulation, *J. Phys. Oceanogr.*, *37*, 1918–1938.

Durack, P. J., and S. E. Wijffels (2010), Fifty-year trends in global ocean salinities and their relationship to broad-scale warming, *J. Clim.*, *23*, 4342–4362.

England, M. H., S. McGregor, P. Spence, G. A. Meehl, A. Timmermann, W. Cai, A. Sen Gupta, M. J. McPhaden, A. Purich, and A. Santoso (2014), Recent intensification of wind-driven circulation in the Pacific and the ongoing warming hiatus, *Nat. Clim. Change*, *4*, 222–227.

Evans, D. G., J. Toole, G. Forget, J. D. Zika, A. C. Naveira Garabato, A. J. G. Nurser, and L. Yu (2017), Recent wind-driven variability in Atlantic water mass distribution and meridional overturning circulation, *J. Phys. Oceanogr.*, *47*, 633–647.

Gao, L., S. R. Rintoul, and W. Yu (2018), Recent wind-driven change in Subantarctic Mode Water and its impact on ocean heat storage, *Nat. Climate Change*, *8*, 58–63.

Gille, S. T. (2002), Warming of the Southern Ocean since the 1950's, *Science*, *295*, 1275–1277.

Good, S. A., M. J. Martin, and N. A. Rayner (2013), EN4: Quality controlled ocean temperature and salinity profiles and monthly objective analyses with uncertainty estimates, *J. Geophys. Res. Oceans*, *118*, 6704–6716.

Gregory, J. M., N. Bouttes, S. M. Griffies, H. Haak, W. J. Hurlin, J. Jungclaus, M. Kelley, W. G. Lee, J. Marshall, A. Romanou, O. A. Saenko, D. Stammer, and M. Winton (2016), The flux-anomaly-forced model intercomparison project (FAFMIP) contribution to CMIP6: Investigation of sea-level and ocean climate change in response to CO2 forcing, *J. Atmos. Oceanic Technol.*, *9*, 3993–4017.

Häkkinen, S., P. B. Rhines, and D. L. Worthen (2016), Warming of the global ocean: Spatial structure and water mass trends, *J. Clim.*, *29*, 4949–4963.

Holte, J., L. D. Talley, J. Gilson, and D. Roemmich (2017), An Argo mixed layer climatology and database, *Geophys. Res. Lett.*, *44*, 5618–5626.

Huang, R. X. (2015), Heaving modes in the world oceans, *Clim. Dyn.*, *45*, 3563–3591.

Johnson, G. C. (2006), Generation and initial evolution of a mode water θ–S anomaly, *J. Phys. Oceanogr.*, *36*, 739–751.

Khatiwala, S., F. Primeau, and T. Hall (2009), Reconstruction of the history of anthropogenic CO2 concentrations in the ocean, *Nature*, *462*, 346–349.

Kolodziejczyk, N., and F. Gaillard (2012), Observation of spiciness interannual variability in the Pacific pycnocline, *J. Geophys. Res.*, *117*, C12,018.

Lago, V., S. E. Wijffels, P. J. Durack, J. A. Church, N. L. Bindoff, and S. J. Marsland (2016), Simulating the role of surface forcing on observed multidecadal upper ocean salinity changes, *J. Clim.*, *29*, 5575–5588.

Levitus, S., J. I. Antonov, T. P. Boyer, O. K. Baranova, H. E. Garcia, R. A. Locarnini, A. V. Mishonov, J. R. Reagan, D. Seidov, E. S. Yarosh, and M. M. Zweng (2012), World ocean heat content and thermosteric sea level change (0–2000 m), 1955–2010, *Geophys. Res. Lett.*, *39*, L10,603.

Luo, Y., L. M. Rothstein, R.-H. Zhang, and A. J. Busalacchi (2005), On the connection between South Pacific subtropical spiciness anomalies and decadal equatorial variability in an ocean general circulation model, *J. Geophys. Res.*, *110*, C10,002.

Luyten, J. R., J. Pedlosky, and H. Stommel (1983), The ventilated thermocline, *J. Phys. Oceanogr.*, *13*, 292–309.

Marshall, J., A. J. G. Nurser, and R. G. Williams (1993), Inferring the subduction rate and period over the North Atlantic, *J. Phys. Oceanogr.*, *23*, 1315–1329.

McCartney, M. S. (1977), Subantarctic Mode Water, in *A Voyage of Discovery (Suppl. to Deep Sea Res.), edited by M. Angel*, pp. 103–185, Pergamon, New York.

McCartney, M. S. (1982), The subtropical recirculation of Mode Waters, *J. Mar. Res.*, *40*, 427–464.

Piecuch, C. G., R. M. Ponte, C. M. Little, M. W. Buckley, and I. Fukumori (2017), Mechanisms underlying recent decadal changes in subpolar North Atlantic ocean heat content, *J. Geophys. Res. Oceans*, *122*, 7181–7197.

Qiu, B., and S. Chen (2012), Multidecadal sea level and gyre circulation variability in the northwestern tropical Pacific Ocean, *J. Phys. Oceanogr.*, *42*, 193–206.

Rhein, M., S. R. Rintoul, S. Aoki, E. Campos, D. Chambers, R. A. Feely, S. Gulev, G. C. Johnson, S. A. Josey, A. Kostianoy, C. Mauritzen, D. Roemmich, L. D. Talley, and F. Wang (2013), *Observations: Ocean, in*, 255-315 pp., Cambridge Univ. Press, Cambridge, U. K., and New York.

Robbins, P. E., J. F. Price, W. B. Owens, and W. J. Jenkins (2000), The importance of lateral diffusion for the ventilation of the lower thermocline in the subtropical North Atlantic, *J. Phys. Oceanogr.*, *30*, 67–89.

Roemmich, D., J. Gilson, R. Davis, P. Sutton, S. Wijffels, and S. Riser (2007), Decadal spinup of the South Pacific subtropical gyre, *J. Phys. Oceanogr.*, *37*, 162–173.

Roemmich, D., J. Church, J. Gilson, D. Montelesan, P. Sutton, and S. Wijffels (2015), Unabated planetary warming and its ocean structure since 2006, *Nat. Climate Change*, *5*, 240–245.

Roemmich, D., J. Gilson, P. Sutton, and N. Zilberman (2016), Multidecadal change of the South Pacific gyre circulation, *J. Phys. Oceanogr.*, *46*, 1871–1883.

Ruddick, B. (1983), A practical indicator of the stability of the water column to double-diffusive activity, *Deep-Sea Res.*, *30*, 1105–1107.

Sallée, J.-B., K. Speer, S. R. Rintoul, and S. Wijffels (2010), Southern Ocean thermocline ventilation, *J. Phys. Oceanogr.*, *40*, 509–529.

Talley, L. D. (1999), Some aspects of ocean heat transport by the shallow, intermediate and deep overturning circulations, in *Mechanisms of Global Climate Change at Millennial Time Scales, Geophys. Monogr. Ser.*, vol. 112, pp. 1–22, edited by P. Clark, R. Webb, and L. Keigwin.

Vaughan, S. L., and R. L. Molinari (1997), Temperature and salinity variability in the deep western boundary current, *J. Phys. Oceanogr.*, *27*, 749–761.

Woods, J. D. (1985), Physics of thermocline ventilation, in *Coupled Atmosphere-Ocean Models*, J. C. J. Nihoul, Ed., Elsevier.

Wu, L., W. Cai, L. Zhang, H. Nakamura, A. Timmermann, T. Joyce, M. J. McPhaden, M. Alexander, B. Qiu, M. Visbeck, P. Chang, and B. Giese (2012), Enhanced warming over the global subtropical western boundary currents, *Nat. Clim. Change*, *2*, 161–166.

Yang, H., G. Lohmann, W. Wei, M. Dima, M. Ionita, and J. Liu (2016), Intensification and poleward shift of subtropical western boundary currents in a warming climate, *J. Geophys. Res.*, *121*, 4928–4945.

Yeager, S. G., and W. G. Large (2004), Late-winter generation of spiciness on subducted isopycnals, *J. Phys. Oceanogr.*, *34*, 1528–1546.

Yeager, S. G., and W. G. Large (2007), Observational evidence of winter spice injection, *J. Phys. Oceanogr.*, *37*, 2895–2919.

Zanna, L., S. Khatiwala, J. M. Gregory, J. Ison, and P. Heimbach (2019), Global reconstruction of historical ocean heat storage and transport, *Proc. Natl. Acad. Sci.*, *116*, 1126–1131.

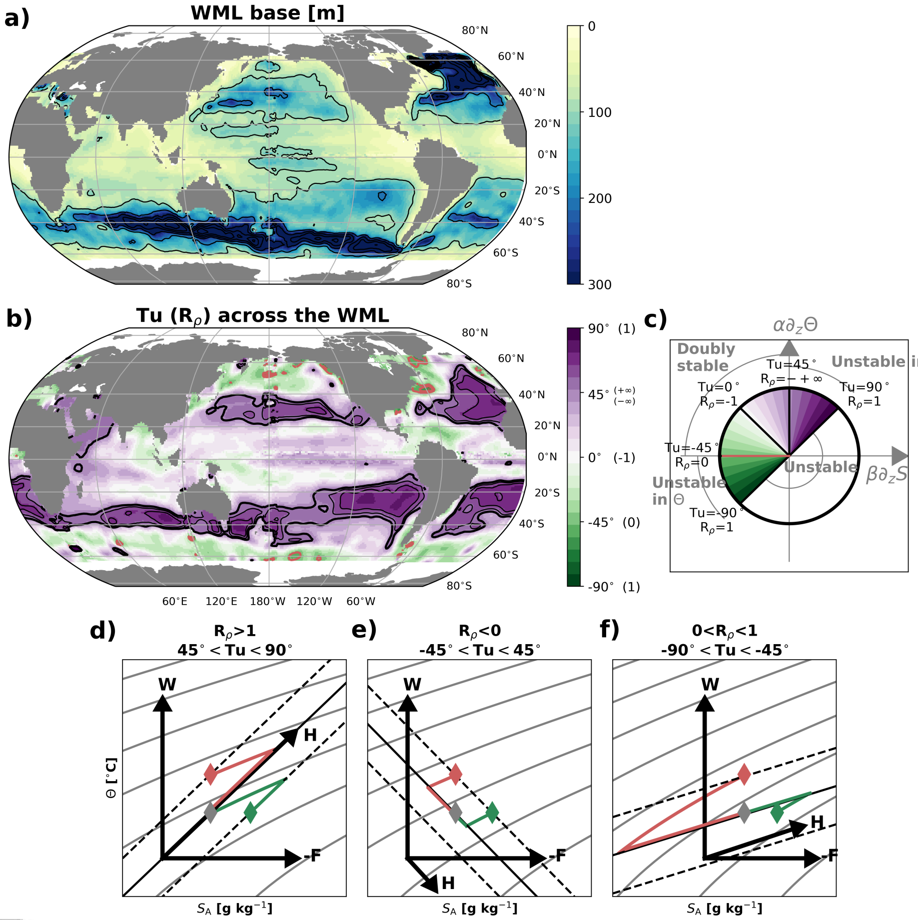

Figure 1. (a) Maximum winter mixed layer depth referred as the WML base. (b) Turner angle across the WML base averaged for the three winter months of each hemisphere. The black lines correspond to Tu=45° (thick line) with an increment every 10°; Tu=-45° is indicated in thick red. The colorbar labels also indicate the equivalent R_ρ in brackets. In (c), Tu and R_ρ are displayed in $\beta\partial_z S$, $\alpha\partial_z\Theta$ coordinates. Θ-S plot for three different R_ρ (after *Bindoff and McDougall* [1994]): (d) warm/salty waters above cool/fresh waters, (e) warm/fresh waters above cool/salty waters, and (f) cool/fresh waters above warm/salty waters. The spice/heave decomposition is described for warming (grey to red diamond) and salinification (grey to green diamond). The three axes of the pure processes [*Bindoff and McDougall*, 1994] are indicated W: warming, F: freshening, and H: heave. The solid black and dashed lines correspond to Θ-S profiles and the grey lines are the isopycnals.

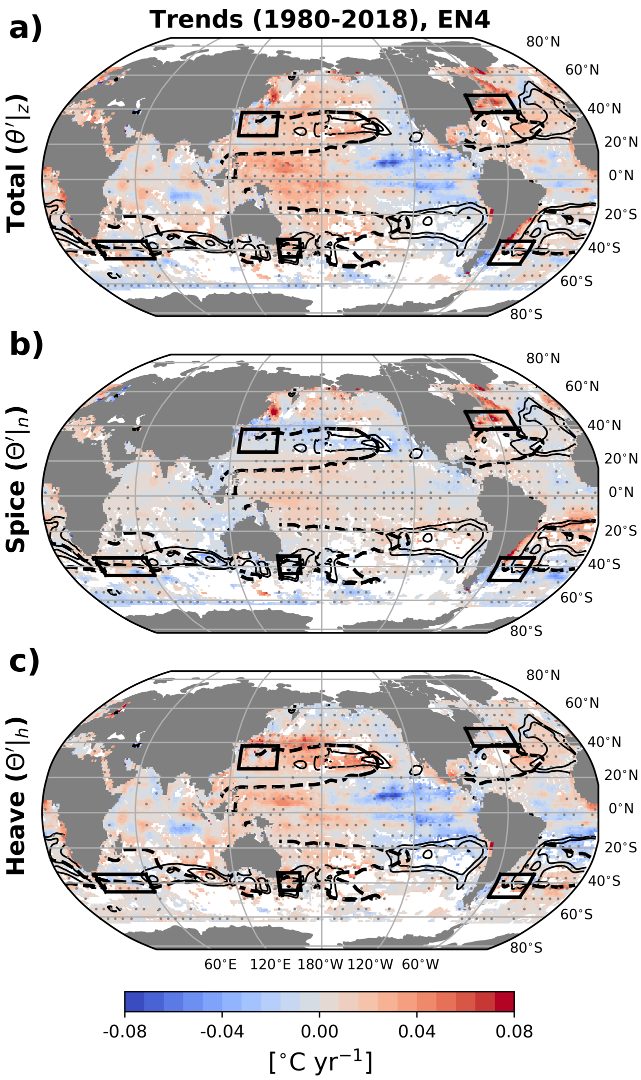

Figure 2. (a) Total, (b) spice and (c) heave components of the temperature trends at the WML base for 1980-2018. Subtropical gyres, western boundary currents and regions with large vertical density compensation in temperature and salinity (Tu>55°) are delimited in thick dashed black contours, black rectangles and thin black contours, respectively. Stippling indicates where the trends are significant with a 95% confidence interval. White regions denote sparse data coverage over the pre-Argo period (Section 3.4).

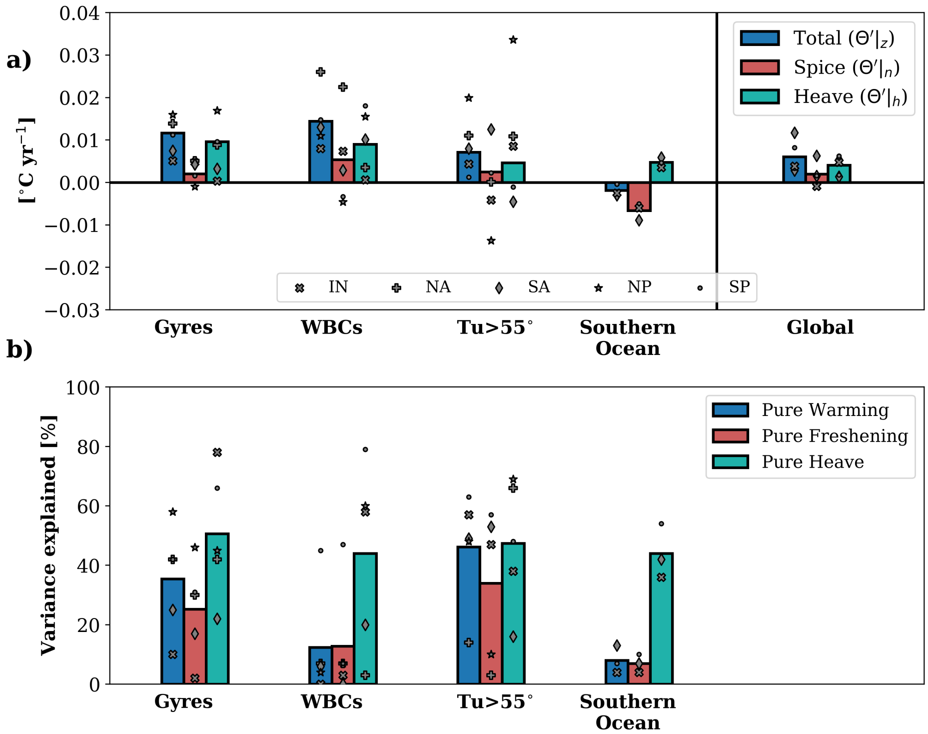

Figure 3. (a) Total (blue) temperature trends [°C yr^{-1}], its spice (red) and heave (green) components averaged over the regions defined in Fig. 2 with the black signs corresponding to each basin. (b) Variance explained by the three pure processes (pure warming, pure freshening, and pure heave) averaged over the regions defined in Fig. 2 using the total, the spice, and the heave trends of Θ and S.

Figure 1.

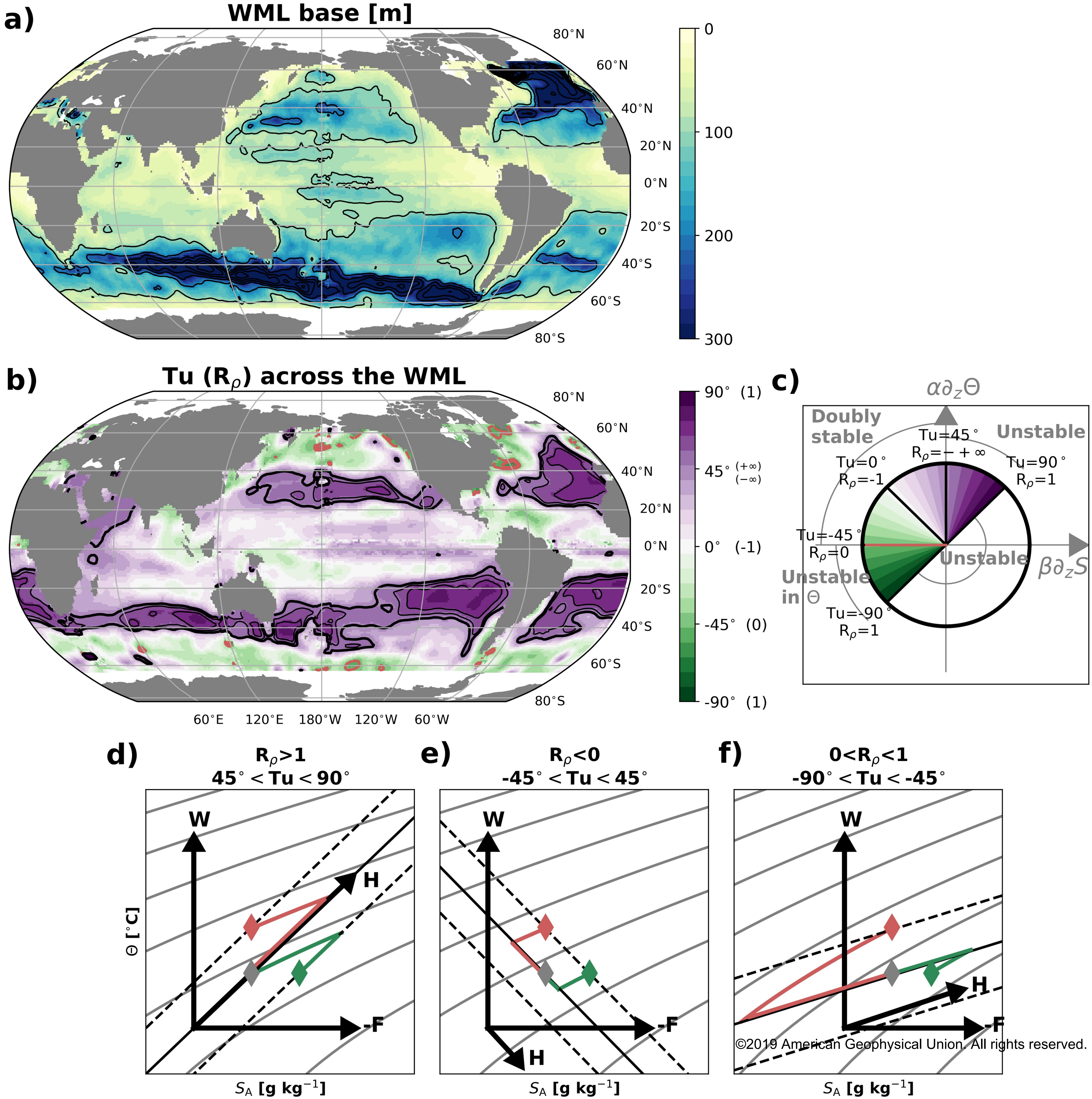
a)
WML base [m]
b)
Tu (R$_\rho$) across the WML
c)
$\alpha\partial_z\Theta$
$\beta\partial_z S$
Doubly stable
Unstable in S
Unstable in Θ
Unstable
Tu=45°
R$_\rho$=−+∞
Tu=0°
R$_\rho$=-1
Tu=90°
R$_\rho$=1
Tu=-45°
R$_\rho$=0
Tu=-90°
R$_\rho$=1
d)
R$_\rho$>1
45° < Tu < 90°
e)
R$_\rho$<0
-45° < Tu < 45°
f)
0<R$_\rho$<1
-90° < Tu < -45°
W
H
-F
Θ [°C]
S_A [g kg^{-1}]

Figure 2.

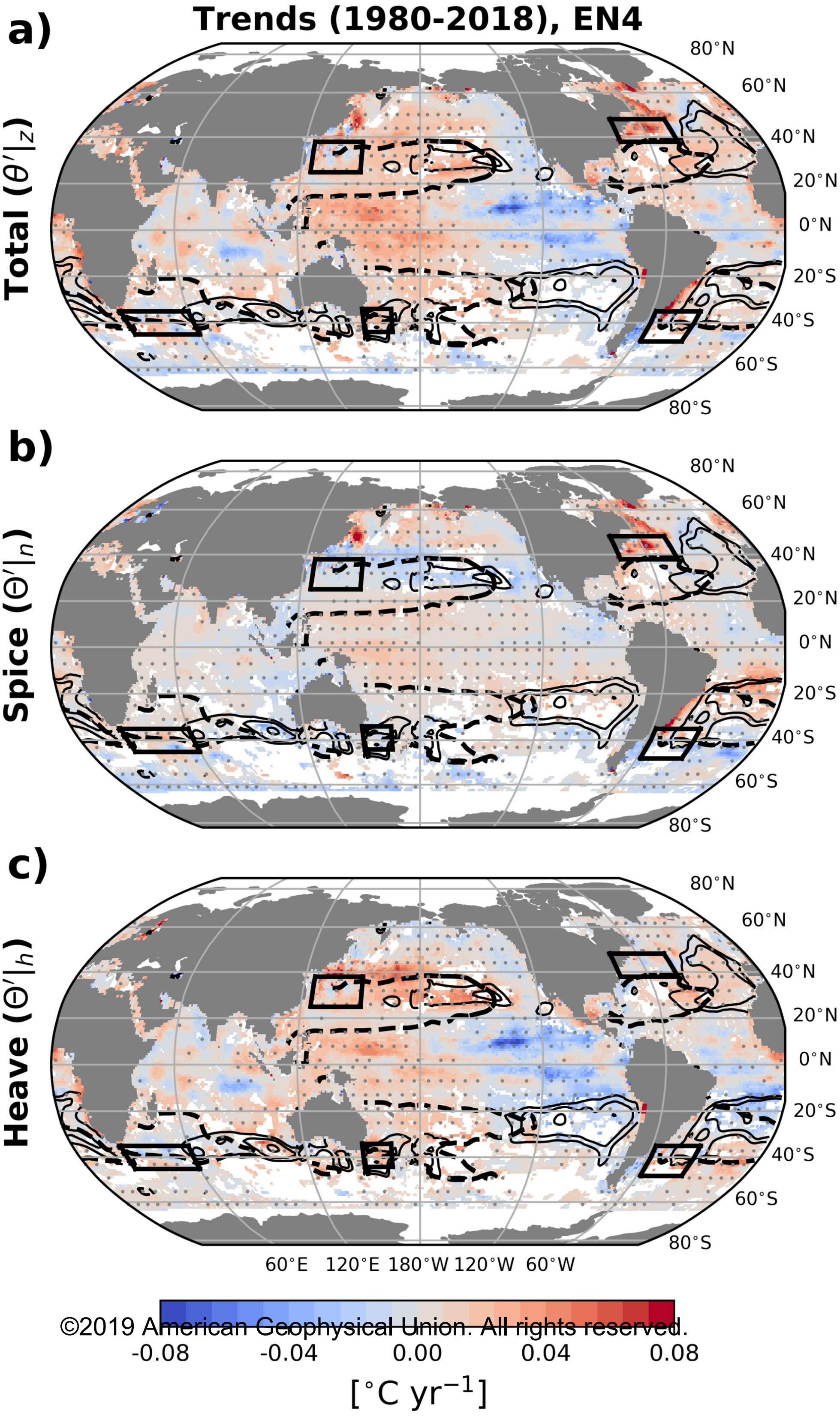

a)
Trends (1980-2018), EN4
Total ($\theta'|_z$)
b)
Spice ($\Theta'|_n$)
c)
Heave ($\Theta'|_h$)
80°N
60°N
40°N
20°N
0°N
20°S
40°S
60°S
80°S
60°E
120°E
180°W
120°W
60°W
-0.08
-0.04
0.00
0.04
0.08
[°C yr^{-1}]

Figure 3.

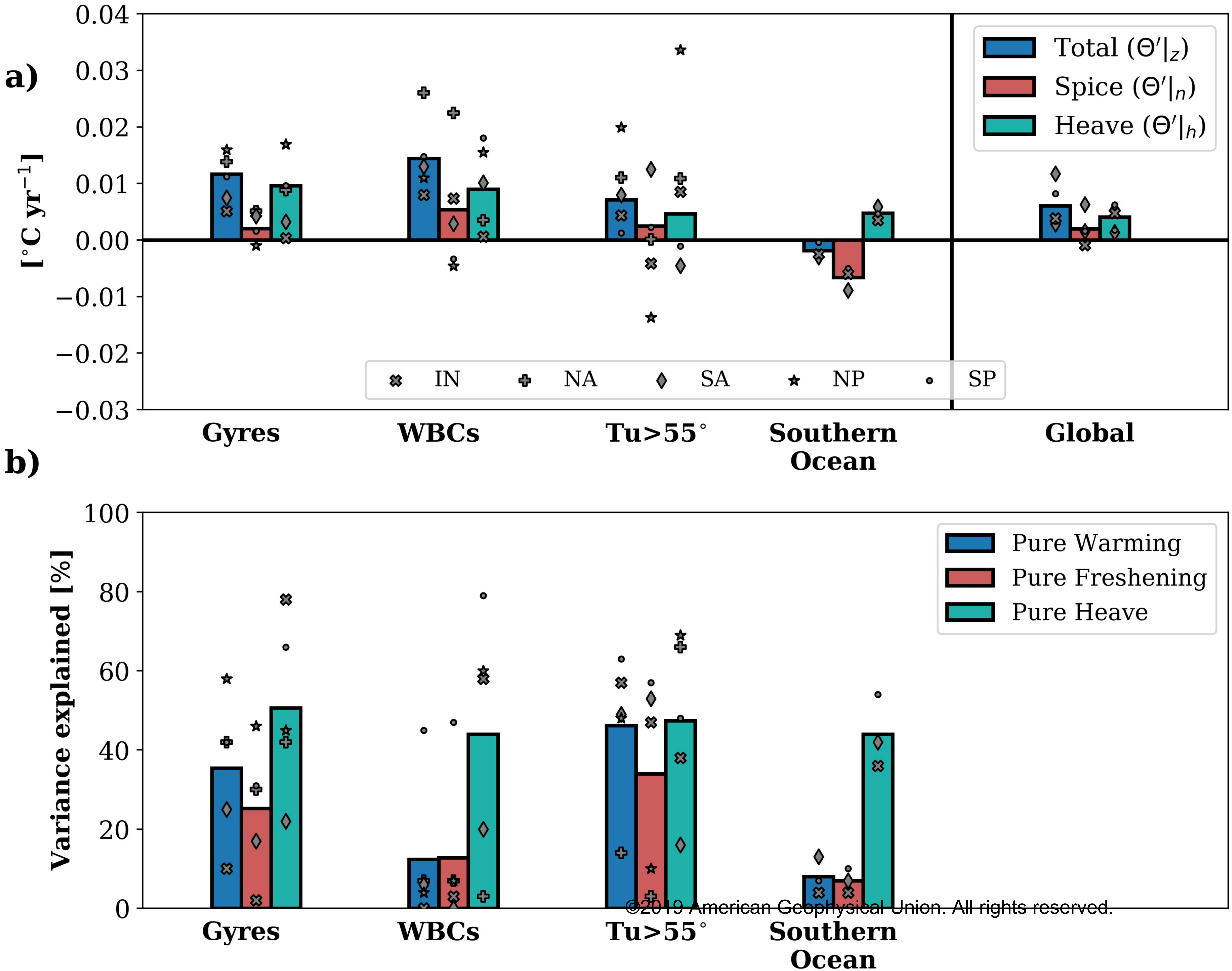
a)
b)
0.04
0.03
0.02
0.01
0.00
−0.01
−0.02
−0.03
[°C yr^{-1}]
Total ($\Theta'|_z$)
Spice ($\Theta'|_n$)
Heave ($\Theta'|_h$)
IN
NA
SA
NP
SP
Gyres
WBCs
Tu>55°
Southern Ocean
Global
100
80
60
40
20
0
Variance explained [%]
Pure Warming
Pure Freshening
Pure Heave